Anatomy of the β-branching enzyme of polyketide biosynthesis and its interaction with an acyl-ACP substrate

Finn P. Maloney[a,b], Lena Gerwick[c], William H. Gerwick[c,d], David H. Sherman[a,e,f,g], and Janet L. Smith[a,h,1]

[a]Life Sciences Institute, University of Michigan, Ann Arbor, MI 48109; [b]Chemical Biology Doctoral Program, University of Michigan, Ann Arbor, MI 48109; [c]Center for Marine Biotechnology and Biomedicine, Scripps Institution of Oceanography, University of California, San Diego, La Jolla, CA 92093; [d]Skaggs School of Pharmacy and Pharmaceutical Sciences, University of California, San Diego, La Jolla, CA 92093; [e]Department of Medicinal Chemistry, University of Michigan, Ann Arbor, MI 48109; [f]Department of Chemistry, University of Michigan, Ann Arbor, MI 48109; [g]Department of Microbiology and Immunology, University of Michigan, Ann Arbor, MI 48109; and [h]Department of Biological Chemistry, University of Michigan, Ann Arbor, MI 48109

Edited by Chaitan Khosla, Stanford University, Stanford, CA, and accepted by Editorial Board Member Gregory A. Petsko July 23, 2016 (received for review May 11, 2016)

Alkyl branching at the β position of a polyketide intermediate is an important variation on canonical polyketide natural product biosynthesis. The branching enzyme, 3-hydroxy-3-methylglutaryl synthase (HMGS), catalyzes the aldol addition of an acyl donor to a β-keto-polyketide intermediate acceptor. HMGS is highly selective for two specialized acyl carrier proteins (ACPs) that deliver the donor and acceptor substrates. The HMGS from the curacin A biosynthetic pathway (CurD) was examined to establish the basis for ACP selectivity. The donor ACP (CurB) had high affinity for the enzyme (K_d = 0.5 μM) and could not be substituted by the acceptor ACP. High-resolution crystal structures of HMGS alone and in complex with its donor ACP reveal a tight interaction that depends on exquisite surface shape and charge complementarity between the proteins. Selectivity is explained by HMGS binding to an unusual surface cleft on the donor ACP, in a manner that would exclude the acceptor ACP. Within the active site, HMGS discriminates between pre- and post-reaction states of the donor ACP. The free phosphopantetheine (Ppant) cofactor of ACP occupies a conserved pocket that excludes the acetyl-Ppant substrate. In comparison with HMG-CoA (CoA) synthase, the homologous enzyme from primary metabolism, HMGS has several differences at the active site entrance, including a flexible-loop insertion, which may account for the specificity of one enzyme for substrates delivered by ACP and the other by CoA.

natural products | polyketide synthase | curacin | HMG synthase | acyl carrier protein

Polyketides are a large and chemically diverse group of natural products that includes many pharmaceuticals with a broad range of biological activities and applications as antibiotics, antifungals, antiinflammatory drugs, and cancer chemotherapeutic agents (1). Polyketide synthase (PKS) biosynthetic pathways are subjects of efforts to engineer diversification of natural products in pursuit of pharmaceutical leads and compounds of industrial importance (2). They are rich sources for development of chemoenzymatic catalysts based on PKS enzymes with unusual catalytic activities.

Modular type I PKS pathways, among the most versatile of nature's systems, are biosynthetic assembly lines composed of modules that act in a defined sequence to produce complex products with a variety of functional groups and chiral centers. Each module is a set of fused catalytic domains that extend and modify a polyketide intermediate. Biosynthesis proceeds from intermediates tethered to acyl carrier protein (ACP) domains via a thioester link to a phosphopantetheine (Ppant) cofactor. A ketosynthase (KS) domain catalyzes extension of the intermediate, and subsequent modification domains typically catalyze reduction and/or methylation of the β-keto (3-keto) extension product. Beyond the enzymes for these core reactions, many PKS pathways also include other catalytic functionality. Among the most interesting of these noncanonical capabilities is alkylation at the β position by a set of β-branching enzymes (3). A 3-hydroxymethylglutaryl (HMG) synthase enzyme (HMGS) catalyzes the key branch-incorporation step, generating a β-hydroxy, β-carboxyalkyl acyl-ACP (Fig. 1*A*). The final structure of a β-branch depends on the carboxyalkyl group and the series of enzymatic steps that tailor the initial branch generated by HMGS (3).

The natural product curacin A, produced by the marine cyanobacterium *Moorea producens* (4), has cytotoxic activity and has been explored as an anticancer agent (5). The hybrid PKS/NRPS (nonribosomal peptide synthetase) pathway for curacin A contains an abundance of unique enzymes that install distinctive functional groups (6), including a cyclopropane ring formed by a surprising variation of the β-branching process (7). In curacin A β-branching, the initial HMG-ACP intermediate undergoes chlorination, dehydration, and decarboxylation before a reductive ring-closing reaction generates the final cyclopropane group (7) (Fig. S1).

HMGS is a homolog of the KS extension enzyme in PKS pathways, but it is more closely related to HMG-CoA (CoA) synthase (HMGCS), an enzyme of primary metabolism in the mevalonate-dependent isoprenoid pathway, where it acts directly before HMG-CoA reductase (8). HMGCS generates HMG-CoA from acetyl-CoA and acetoacetyl-CoA by an aldol addition (Fig. S1*B*). The acetyl group is transferred to a catalytic cysteine, then

Significance

Polyketides are a chemically diverse class of natural products with broad pharmaceutical applications. β-Branching in modular polyketide synthase pathways contributes to this diversity by introducing alkyl branches into polyketide intermediates, ranging from simple methyl groups to more unusual structures, including the curacin A cyclopropane ring. Branching replaces the β-carbonyl of a polyketide intermediate, which is more commonly reduced and/or methylated. Furthermore, β-branching is catalyzed by cassettes of standalone enzymes and is targeted to a specific point in a polyketide synthase PKS pathway by specialized acyl carrier proteins (ACPs). In these structural studies, we have begun to elucidate the mechanisms of ACP selectivity by the initiating enzyme of β-branching. This work may be essential for rational efforts to diversify polyketides using unnatural β-branching schemes.

Author contributions: F.P.M. and J.L.S. designed research; F.P.M. performed research; L.G., W.H.G., and D.H.S. contributed new reagents/analytic tools; F.P.M. and J.L.S. analyzed data; and F.P.M. and J.L.S. wrote the paper.

The authors declare no conflict of interest.

This article is a PNAS Direct Submission. C.K. is a Guest Editor invited by the Editorial Board.

Data deposition: The atomic coordinates and structure factors have been deposited in the Protein Data Bank, www.pdb.org (PDB ID codes 5KP5, 5KP6, 5KP7, and 5KP8).

[1]To whom correspondence should be addressed. Email: JanetSmith@umich.edu.

This article contains supporting information online at www.pnas.org/lookup/suppl/doi:10.1073/pnas.1607210113/-/DCSupplemental.

www.pnas.org/cgi/doi/10.1073/pnas.1607210113

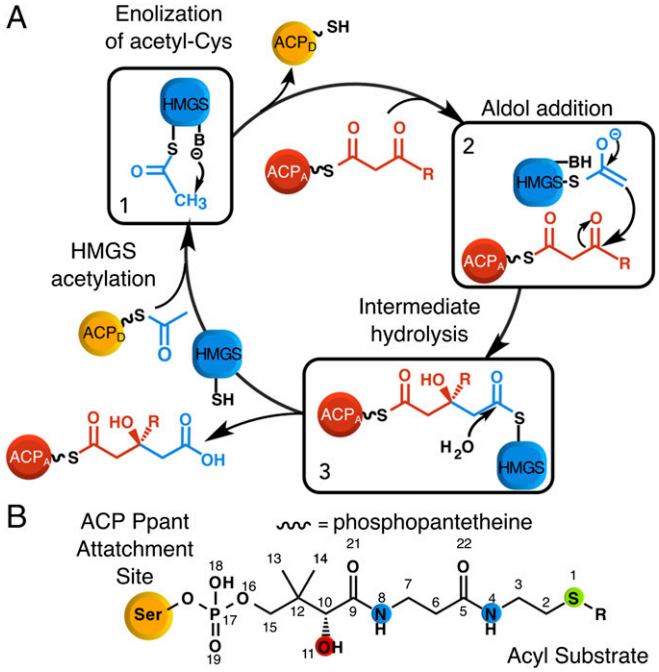

Fig. 1. HMGS reaction. (*A*) Reaction steps. (*1*) ACP_D transfers an acetyl group to HMGS Cys114 and Glu82 deprotonates the acetyl group; (*2*) the resulting enolate nucleophile attacks acetoacetyl-ACP_A; (*3*) the HMG-ACP_A product is hydrolyzed from Cys114. R indicates the polyketide intermediate (methyl in curacin A biosynthesis). (*B*) Structure of the Ppant cofactor (represented as a squiggle symbol in *A*).

deprotonated by a conserved glutamate. The resulting enolate nucleophile attacks the β-carbonyl of the second substrate, acetoacetyl-CoA. The covalent enzyme-product complex is hydrolyzed to release HMG-CoA. HMGCS is well characterized, including crystal structures of complexes between the enzyme and its product, substrates, and inhibitors (9–14).

The HMGS and HMGCS reactions (Fig. 1) are analogous and, in the case of the curacin A HMGS (CurD), have identical acyl substrates that are tethered to distinct ACPs and not to CoA. Whereas HMGCS distinguishes acetyl-CoA and acetoacetyl-CoA based on the acyl group and the acetylation status of the catalytic cysteine, HMGS also displays ACP selectivity: a standalone acetyl "donor" ACP (ACP_D), and an acetoacetyl-like "acceptor" ACP (ACP_A) bearing the polyketide intermediate within a specific module of the PKS pathway (15, 16). HMGS enzymes are highly selective for acetoacetyl-ACP_A and acetyl-ACP_D, and do not react with CoA substrates (15–17). At the sequence level, the donor and acceptor ACPs clade separately from each other and from nonbranch ACPs from the same pathways (15, 18). Thus, by selecting for the correct acyl-ACPs, HMGS prevents the formation of aberrantly branched metabolites.

The basis of ACP selectivity by HMGS is unknown, and detailed views of ACP interactions with PKS enzymes are few. The homologous KS extension enzymes distinguish their cognate donor and acceptor ACPs through two active site entrances (19) in interactions facilitated by fusion or noncovalent interaction of appended docking domains (20, 21), which are absent in HMGS. HMGS selectivity for ACP_A and ACP_D presumably originates from distinguishing features of each ACP that result in different modes of interaction with HMGS. Here we present the biochemical characterization of the curacin A HMGS (CurD) and the interaction with its cognate ACP_D (CurB). Crystal structures of HMGS and of complexes with ACP_D reveal a striking shape complementarity between the proteins and specific charge interactions that orient the Ppant cofactor in the HMGS active site. Pre- and postacetyl transfer states of Ppant capture sequential views of the catalytic cycle. The results are a detailed benchmark of high-affinity enzyme-ACP interactions that advance our understanding of enzyme selectivity for carrier proteins.

Results

CurD HMGS Activity. Purified, recombinant ACP_D (CurB) and the second cognate ACP_A from the CurA tandem ACP_A tridomain (Fig. S1) were acylated in vitro. Recombinant CurD HMGS converted 83% of equimolar acetyl-ACP_D and acetoacetyl-ACP_A to HMG-ACP_A in a 10-min reaction at 25 °C (Table 1). Reaction progress was monitored by LC-MS using the acyl-Ppant ejection assay (22) (Fig. S2 and Table S1). We detected no conversion of acetoacetyl-ACP_A to HMG-ACP_A when the catalytic Cys114 was substituted with serine (Table 1). The C114S substitution also prevented acetyl transfer from acetyl-ACP_D (Table S2).

HMGS Structure. A triple alanine HMGS variant (K344A/Q345A/Q347A, $HMGS_{AAA}$) was used for all crystal structures and had catalytic activity indistinguishable from the WT (Table 1). The 2.1-Å crystal structure in space group $P3_121$ (Table S3) was solved by molecular replacement. HMGS is dimeric in solution and in the crystal structure, where the asymmetric unit consists of one subunit (Fig. 2). The catalytic amino acids Glu82, Cys114, and His250 (Figs. S3*A* and S4*A*) are identically positioned in HMGS and HMGCS, and the overall folds are similar (RMSD of 2.03 Å for 368 Cα atoms). Striking differences occur at the active site entrance and the dimer interface. A disordered loop (HMGS residues 149–163) near the active site encompasses a conserved insertion in HMGS (residues 155–164) relative to HMGCS (Fig. S3*A*). An adjacent loop at the subunit interface (residues 203–210) has a different conformation than the analogous loop in HMGCS. The HMGS 203–210 loop forms hydrophobic contacts with the partner subunit that involve several residues conserved among HMGS but not HMGCS.

HMGS-ACP_D Complex. We tested the ACP selectivity of the curacin A HMGS in experiments where acyl groups were mismatched with ACP_D or ACP_A (Table 1 and Fig. S2). ACP_A was not a surrogate acetyl donor, as we detected no conversion of acetyl-ACP_A + acetoacetyl-ACP_A to HMG-ACP_A. In contrast, ACP_D was a weak surrogate acceptor with threefold-reduced conversion of acetyl-ACP_D + acetoacetyl-ACP_D to HMG-ACP_D relative to the natural partners. Thus, HMGS had greater selectivity for the donor ACP than for the acceptor. To investigate the structural basis of ACP selectivity, we pursued structures of HMGS complexes with ACP_A and ACP_D.

The HMGS active site entrance and surrounding surface were unhindered by crystal contacts, and we captured complexes of HMGS with apo-ACP_D, holo-ACP_D, and acetyl-ACP_D by cocrystallization (Fig. 3 and Table S3). The ACP_D was well ordered at the HMGS active site entrance, made no lattice contacts, and contacted neither the partner subunit of the HMGS dimer nor its bound ACP_D. The holo-ACP_D Ppant had clear electron density in the active site (Fig. 4*A* and Fig. S4*B*) yet formed only a few interactions, including the phosphate to HMGS Arg33 and ACP_D Arg42, which was also salt-bridged to HMGS Asp214 (Fig. 3 *B* and *C*). The Ppant-Arg42-Asp214 network is specific to ACP_D-HMGS pairs (Fig. S3), but the Arg33-Ppant interaction also occurred in HMGCS-CoA complexes (9, 11). Ppant binding induced ordering of amino acids 159–163 in the HMGS disordered loop, forming a 3_{10} helix with hydrogen bonds of Phe163 and Ser167 to the Ppant (Fig. 3*B*). The Ppant thiol occupies a relatively hydrophobic "thiol pocket" (conserved amino acids Ser216, Leu217, Tyr220, Pro252, Met256 and Tyr326) and is hydrogen bonded to the Ser216 hydroxy group (Fig. 3*B*). An extensive network of hydrogen bonds involving Ser216, Tyr220, Tyr326 and conserved Asp200 maintains the structure of the thiol pocket.

In the holo-ACP_D/HMGS structure, the Ppant and Cys114 thiol groups are too far apart (7.9 Å) for the acetyl-transfer step of HMGS catalysis (Fig. 4*A*). This distal Ppant position was also occupied in crystals grown from acetyl-ACP_D + HMGS, with no

Table 1. HMGS activity and ACP_D affinity

Sample	HMGS activity (%)*	K_d (apo-ACP_D) (μM)†	K_d (holo-ACP_D) (μM)
HMGS and crystallization variant‡			
WT	82.8 ± 0.3	1.1 ± 0.1	0.5 ± 0.2
AAA‡	87 ± 1	—	—
Mismatched acyl-ACP substrates§			
ACP_D as donor and acceptor	29 ± 2	—	—
ACP_A as donor and acceptor	ND	—	—
HMGS active site substitutions			
C114S	ND	—	—
P166A	88.1 ± 0.3	—	—
S167A	95.5 ± 0.3	—	—
ACP_D/HMGS interface substitutions			
ACP_D			
R42A	95.7 ± 0.2	—	—
HMGS			
R33A	ND	6.9 ± 0.7	8 ± 2
R33D	2 ± 3	29 ± 3	25 ± 3
D214A	86 ± 8	10.9 ± 0.9	9 ± 2
D214R	45 ± 4	17 ± 5	11 ± 3
D222A	27 ± 1	28 ± 2	1.5 ± 0.6
D222R	17 ± 1	34 ± 2	5 ± 1
E225A	55 ± 3	90 ± 4	—
E225R	8 ± 1	68 ± 5	12 ± 1
R266A	56 ± 1	110 ± 10	17 ± 2
R266E	26 ± 1	180 ± 10	17 ± 5

ND, no product detected; —, indicated where the experiment was not performed for the indicated sample.

*Conversion of equimolar acetyl-ACP_D and acetoacetyl-ACP_A to HMG-ACP_A in a 10-min reaction at 25 °C. Each value corresponds to the average of three measurements.

†Affinities were measured by fluorescence polarization using labeled ACP_D. Each value corresponds to the average of three measurements.

‡All crystal structures were of the $HMGS_{AAA}$ variant (K343A/Q344A/Q346A). Cys114 is the catalytic nucleophile.

§In each reaction, either ACP_D or ACP_A was loaded with both acyl substrates, and equimolar quantities of acetyl-ACP and acetoacetyl-ACP were used.

density for an acetyl at either the Ppant or Cys114 (Fig. 4*B* and Table S3). The acetyl group of acetyl-ACP_D was apparently transferred to Cys114 and subsequently hydrolyzed during crystallization (2–3 d) (Table S2). We propose that the distal Ppant position represents a post acetyl-transfer state. Nonproductive loss of the acetyl-CoA donor in absence of the acetoacetyl-CoA acceptor has also been reported for HMGCS (23).

To trap an acetyl-ACP_D complex, we cocrystallized the inactive $HMGS_{C114S}$ with acetyl-ACP_D, resulting in multiple positions for the Ppant terminus (Fig. 4*D*), including the previously identified distal holo-Ppant position, again lacking density for an acetyl group. A second position was interpreted from a new strong density (15σ) near Ser114 that could represent acetyl-Ppant (Fig. 4*D*). Two experiments validated the interpretation of the second proximal acetyl-Ppant position, as its density was discontinuous with the rest of the Ppant. We solved the structure of holo-ACP_D/$HMGS_{C114S}$, yielding density in the distal Ppant position and no density in the Ser114-proximal position, establishing that the new density was not due to the C114S substitution (Fig. 4*C* and Table S3). To distinguish whether the density near Ser114 was due to free acetate or the acetyl-Ppant terminus, we used anomalous scattering to identify atomic positions of S atoms. Data were recorded at an X-ray energy of 7.0 keV from acetyl-ACP_D/$HMGS_{C114S}$ cocrystals, yielding anomalous difference electron density for the Ppant S in both the distal site and at the site proximal to Ser114 (Fig. 4*D* and Table S3). A similar experiment with $HMGS_{C114S}$ crystals (no ACP_D) lacked anomalous difference electron density near Ser114. Thus, we conclude that during crystallization some of the acetyl-ACP_D hydrolyzed spontaneously, and the remaining acetyl-Ppant was adjacent to the nucleophilic side chain (C114S), defining a preacetyl-transfer position.

ACP_D/HMGS Interface. The interacting surfaces of ACP_D and HMGS are complementary in shape and charge (Fig. 3 *C* and *D* and Fig. S6 *A* and *B*). The primary contact is between the N-terminal half of HMGS helix α8 (Fig. 3) and an ACP_D cleft between the Ppant-Ser39 and helix III. On the ACP_D surface, conserved basic residues form a strongly electropositive region, which is separated from an electronegative region by a hydrophobic stripe (Fig. S6). We compared the surface features of other ACPs in complexes with cognate enzymes (24–29) to ACP_D (Fig. S6). Positive and negative surface regions are typical of PKS ACPs (Fig. S6 *B–E*), whereas fatty acid synthase (FAS) ACPs are highly electronegative (Fig. S6 *F–I*). Among PKS ACPs, ACP_D has two distinctive features: a strongly electropositive region and a cleft that is complementary to a conserved hydrophobic patch (Fig. 3*D*) (Leu217, Leu218) on the outer surface of HMGS helix α8. The analogous surface of the HMGCS helix is polar.

We evaluated several salt bridges in the ACP_D-HMGS interface by mutagenesis and, for each variant, measured HMGS activity and ACP_D affinity (Table 1 and Figs. S2 and S5). Each of the HMGS charged residues (Arg33, Asp214, Asp222, Glu225, and Arg266) was substituted with alanine and an oppositely charged amino acid. Affinities were measured by fluorescence anisotropy with a fluorophore-conjugated ACP_D. The HMGS K_d was 1.1 μM for apo-ACP_D and 0.5 μM for holo-ACP_D, indicating significant protein-protein affinity and a twofold contribution from the Ppant cofactor. Asp222, Glu225, and Arg266 are involved in only the protein-protein interface and do not contact the Ppant (Fig. 3*C*). Correspondingly, substitutions to these residues had a greater impact on the affinity of apo-ACP_D than holo-ACP_D. Substitutions to phosphate-interacting Arg33 and Asp214 resulted in equal affinities for holo and apo-ACP_D.

The effect of the HMGS substitutions on activity did not show a clear pattern for Ppant-interacting and protein-protein contact residues. The Arg33 variants had little or no activity, suggesting that the Arg33 may orient Ppant in the active site. In contrast, substitutions to Asp214 did not significantly affect activity. To further test the importance of HMGS-Ppant interactions, we

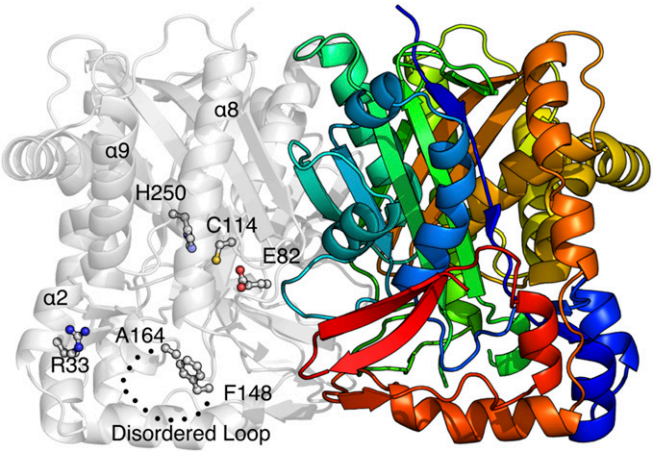

Fig. 2. CurD HMGS structure. Within the dimer, the right-hand subunit is colored by sequence from the blue N terminus to the red C terminus. Key residues are shown in ball-and-stick on the gray left monomer, including the catalytic Cys114, Glu82, and His250. Phe148 and Ala164 are the boundaries of the 15-residue disordered loop at the active site entrance. The basic side chain of Arg33 interacts with the Ppant phosphate and is conserved in HMGCS sequences. A dotted line denotes the disordered loop region connecting Phe148 to Ala164.

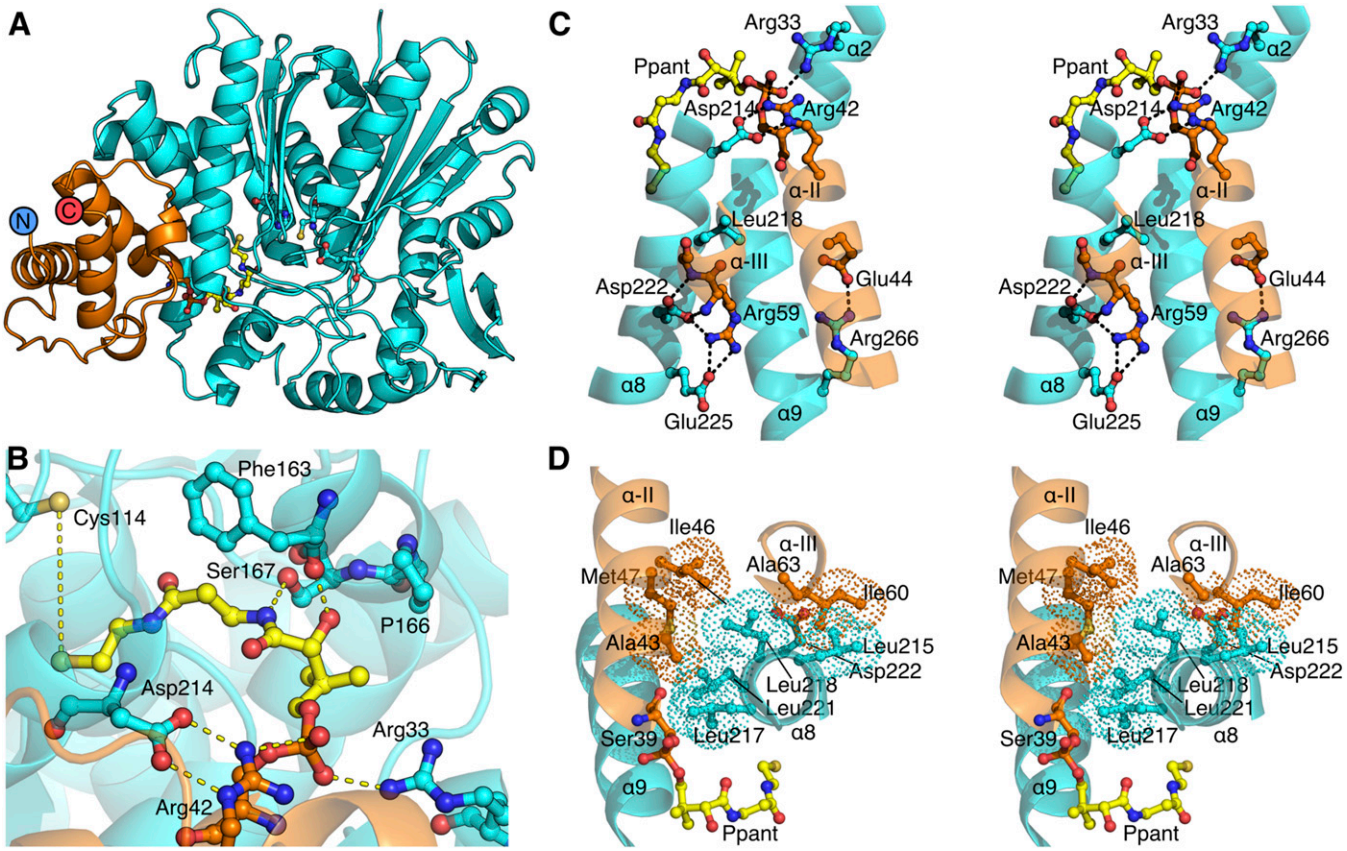

Fig. 3. HMGS interaction with the donor ACP. (*A*) ACP_D (orange)/HMGS (cyan) complex. Ppant (yellow) and catalytic residues shown are in ball-and-stick form. (*B*) Ppant in the HMGS active site. Dashed yellow lines represent hydrogen bonds and the long separation of Ppant and Cys114 thiol groups. (*C*) Stereoview of charged contacts in the HMGS-ACP_D interface. (*D*) Stereoview of hydrophobic contacts between ACP_D and HMGS. HMGS helices are numbered as in Fig. 2, and ACP_D helices are labeled by Roman numerals. Helices in *C* and *D* are transparent for clarity.

made alanine substitutions to Ser167 and to Pro166, which we hypothesized would increase helicity of Phe163 and prevent its carbonyl from interacting with Ppant. Despite the conservation of these residues, both variants had similar activity to WT HMGS, suggesting their interaction with Ppant may be unimportant for the acetylation step of the HMGS mechanism.

Substitutions to charged side chains in the protein-protein interface caused modest reductions in HMGS activity that were not correlated with changes in affinity, indicating that HMGS-ACP_D affinity is not limiting in the assay conditions. At each position, the effect of the charge-reversal substitution was more deleterious to HMGS activity (3- to 10-fold) than was the Ala substitution (threefold or less). The greatest effects occurred for charge-reversal substitutions at Asp222 (5-fold) and Glu225 (10-fold). Located on adjacent turns of helix α8 (Fig. 3*C*), Glu225 forms a salt bridge with ACP_D Arg59, and the Asp222 carboxylate "caps" ACP_D helix III, which is an atypical 3_{10} helix in an unusual position in the ACP (Fig. 3). Thus, Asp222 and Glu225 may help orient ACP_D on HMGS, or may be antiselective for ACP_A at this position.

The ACP_D-HMGS interface provides clues about the selectivity of β-branching in the myxovirescin pathway, which generates methyl and ethyl branches with two ACP_D/HMGS pairs (TaB/TaC and the nonstandard TaE/TaF) (30). Each HMGS (TaC and TaF) is selective for its donor ACP (acetyl-TaB and propionyl-TaE) (16). Homology models of the myxovirescin ACP_Ds and HMGSs accounted for the selectivity, as the TaB/TaC pair retains most of the interactions of CurB/CurD, however, at other interacting positions, complementary sequence changes in TaE ACP_D and TaF were incompatible with the noncognate partner.

Discussion

HMGS catalyzes the key reaction of polyketide β-branching, a critical process for chemical diversification in this important class of natural products. The β-branching HMGS of the curacin A biosynthetic pathway exhibits a remarkable selectivity for its donor (ACP_D) and acceptor (ACP_A) substrates (Table 1), like related enzymes (15–17). This selectivity enables proper sequencing of substrates during catalysis and prevents aberrant β-branching by mis-association with other ACPs within the PKS pathway.

The ACP_D-HMGS structures capture the ACP_D Ppant in pre- and postacetyl transfer positions. In the Cys-distal, postacetyl-transfer position, the Ppant thiol was bound deep within a conserved thiol pocket that occludes the acetyl group, whereas the poorly ordered acetyl-Ppant was in the Cys-proximal position (captured in the Ser114 variant). These positions contrast with structures of HMGCS-CoA complexes (9–11, 13, 14) where, in all cases supported by electron density, the Ppant was bound near the distal site with the thiol directed into the active site cavity regardless of its acylation state. Nevertheless, the HMGS and HMGCS active sites are nearly identical, and thus we infer that HMGS and HMGCS have identical stereochemical outcome, generating only S-HMG products.

A major motivation for our study was to investigate how HMGS distinguishes the two ACP substrates. The structures of the ACP_D-HMGS complexes indicate that HMGS excludes ACP_A from the ACP_D site, consistent with the inability of ACP_A to act as an acetyl donor in the reaction (Table 1). ACP_D has a surface shape that is complementary to the HMGS surface and that differs from surfaces of ACP_A and other ACPs. A hydrophobic cleft, due to the unique position of ACP_D helix III, is matched with a hydrophobic ridge on the surface of HMGS helix α8 (amino acids 213–234) and is flanked by polar contacts, including Asp222 on

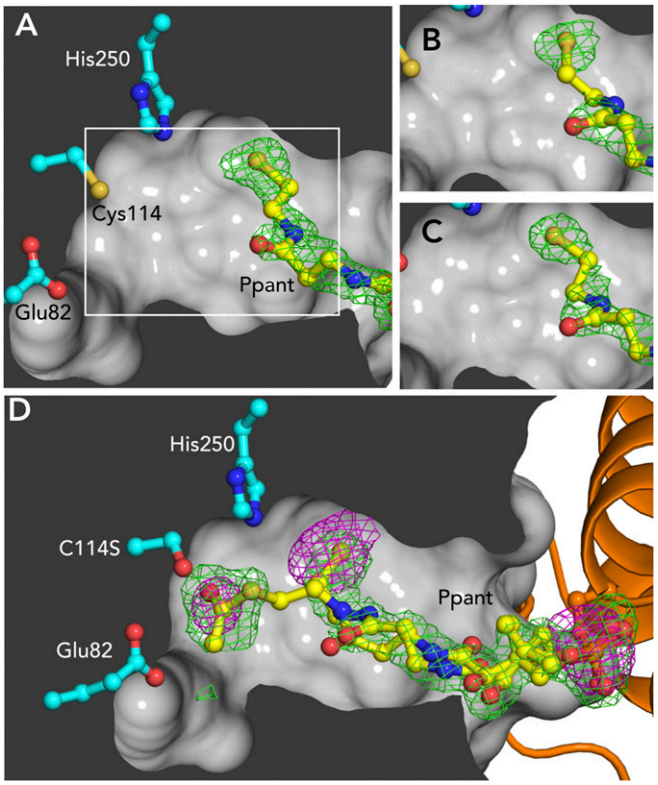

Fig. 4. Acetylation-dependent position of Ppant. Panels show Fo-Fc omit density (3σ, Ser-Ppant omitted, green) for structures of ACP_D-HMGS in different biochemical states crystallized in identical conditions. (*A*) Holo-ACP_D and $HMGS_{WT}$. White box indicates field of view for *B* and *C*. (*B*) Acetyl-ACP_D and $HMGS_{WT}$, showing that the acetyl group has been lost. (*C*) Holo-ACP_D and $HMGS_{C114S}$. (*D*) Acetyl-ACP_D and $HMGS_{C114S}$. Anomalous difference density (3σ, magenta) indicates that S is present in both terminal densities for the Ppant and also shows the Ppant P atom. Atoms are colored as in Fig. 3.

helix α8 with backbone amides at the N terminus of ACP_D helix III. ACP_A has no hydrophobic surface cleft because helix III is in a more typical position. None of the salt bridges between amino acids in ACP_D and HMGS was critical for binding or catalysis when tested by single-residue mutagenesis (Table 1), leading us to conclude that surface complementarity is the dominant factor in the HMGS-ACP_D interface.

ACPs from PKS pathways (18, 24, 25, 31) have distinctive surface charge distributions compared with FAS ACPs (26–29), but in both systems the ACP helix II-III surface interacts with enzymes (Fig. S6). The PKS ACPs have regions of positive surface potential near the point of contact with their cognate enzymes, whereas the analogous surface of the FAS ACPs is negatively charged. The distinctive pattern of negative/neutral/positive surface potential of β-branching ACPs (ACP_D, curacin A, and mupirocin ACP_As) may contribute to HMGS selectivity against the ACPs within PKS modules where the surface potential pattern differs (Fig. S6). The unusual ACP_D helix III, accompanying surface cleft, and striking electrostatics specialize ACP_D for selective interaction with only the β-branching HMGS and KS_{DC} enzymes (Fig. S1). In contrast, ACP_A shuttles substrates to seven enzymes in the curacin A pathway, including β-branching and module enzymes, necessitating a more promiscuous ACP-surface for enzyme interaction.

Catalytic fidelity in a reaction with distinct donor and acceptor substrates is a common problem for HMGS and two homologs: the HMGCS of primary metabolism and the KS domain of modular PKS pathways. The enzymes use different mechanisms of substrate selectivity, although they have analogous active site entrances for their acyl donor substrates. HMGCS has a single binding site for the acetyl-donor and acetoacetyl-acceptor CoAs (10, 14), but excludes the acetyl-CoA donor following acetyl transfer to the enzyme (32). Like HMGS, the PKS KS domain has two ACP substrates but uses separate active site entrances for the donor (upstream module) and acceptor (intramodule) (19). The PKS KS restricts access of each ACP to the appropriate entrance by the module architecture and ACP tethering via fusion or interaction of docking domains (19–21, 33, 34). In contrast, HMGS interacts with two ACPs *in trans*, and robust binding of ACP_D (K_d = 0.5 μM for holo-ACP_D) is not acyl-group dependent. Nor is the ACP_D docking site on HMGS analogous to either of the ACP-KS docking sites observed in cryo-EM maps of a PKS module (19). We find no evidence of a second active site entrance in the HMGS structure (for example, poorly ordered loops that could expose the active site, as in the KS) (19, 21, 35, 36). We conclude that ACP_A and ACP_D insert acyl-Ppant through the same active site entrance, as do the donor and acceptor-CoAs of HMGCS, but that the ACPs interact with different regions of the HMGS surface.

The HMGS flexible loop, which does not exist in either HMGCS or KS, is a prime candidate for ACP_A interaction, as it is adjacent to the active site. A critical question is whether the ACPs engage HMGS simultaneously or sequentially. The affinity of HMGS for ACP_D is tenfold greater than a native docking domain pair (K_d = 0.5 μM vs. 5–25 μM) (20, 21). HMGS has lower affinity for ACP_A than for ACP_D, based on the K_d of 150–200 μM for the bryostatin HMGS and its cognate ACP_A (15). Cooperativity may enhance weak intrinsic ACP_A binding to HMGS because β-branching cassettes typically encode tandem ACP_As, for example the CurA tandem ACP_A tridomain of nearly identical sequences with an additional dimerization element at the C terminus (37). In the HMGS dimer, the two active site entrances are separated by 40–50 Å, a distance that may be spanned by tandem or dimeric ACPs. However, the high activity of HMGS under assay conditions with equal concentrations of ACP_D and single-domain ACP_A implies that HMGS may either promote dissociation of ACP_D, following acetyl transfer to Cys114, or simultaneously engage acetoacetyl-ACP_A to prevent formation of a dead-end complex. Thus, interaction with acetoacetyl-ACP_A could trigger both catalytic and conformational events, including rearrangement of the flexible loop to disengage ACP_D or to widen the active site entrance to accommodate two Ppant cofactors. The possibilities are not resolved by the present structures.

In conclusion, the first structure of an HMG synthase involved in polyketide biosynthesis reveals features that distinguish HMGS from its primary metabolism homolog and allow it to interact selectively with its cognate ACPs. Analysis of the HMGS-ACP_D interface provides insight into HMGS selectivity in other pathways, including those with multiple β-branching functions. The HMGS structures with acetyl and holo-ACP_D provide a unique view of the molecular interactions between a PKS enzyme and its substrate, revealing the mechanism by which HMGS prevents its substrate from adopting a nonproductive orientation in the active site. Finally, the unusual position of helix III in ACP_D is a new structural motif in acyl carrier proteins that can be selectively recognized by specialized enzymes such as HMGS.

Methods

Constructs encoding curacin A HMGS, ACP_D, and ACP_A and variants (Table S4) were expressed in *E. coli* and purified by IMAC and size exclusion chromatography. HMGS activity was assayed by LC-MS with Ppant ejection to detect conversion of acetoacetyl-ACP_A to HMG-ACP_A. HMGS affinity for ACD_D was measured by fluorescence anisotropy using a labeled variant of ACP_D. HMGS and ACP_D/HMGS complexes were crystallized by hanging drop vapor diffusion. X-ray diffraction data were collected at GM/CA at the Advanced Photon Source. Homology models of the myxovirescin HMGS and ACP_Ds were generated using Modeller.

ACKNOWLEDGMENTS. This work was supported by US NIH Grants R01-DK042303 (to J.L.S.), R01-CA108874 (to D.H.S., J.L.S., and W.H.G.), and the Hans W. Vahlteich Professorship (D.H.S.). The GM/CA at APS beamlines are funded in whole or in part with Federal funds from the National Cancer Institute (CA) (ACB-12002) and the National Institute of General Medical Sciences (GM) (AGM-12006). This research used resources of the Advanced Photon Source, a US Department of Energy (DOE) Office of Science User Facility operated for the DOE Office of Science by Argonne National Laboratory under Contract DE-AC02-06CH11357.

1. Cragg GM, Newman DJ (2013) Natural products: A continuing source of novel drug leads. *Biochim Biophys Acta* 1830(6):3670–3695.
2. Weissman KJ (2016) Genetic engineering of modular PKSs: From combinatorial biosynthesis to synthetic biology. *Nat Prod Rep* 33(2):203–230.
3. Calderone CT (2008) Isoprenoid-like alkylations in polyketide biosynthesis. *Nat Prod Rep* 25(5):845–853.
4. Blokhin AV, et al. (1995) Characterization of the interaction of the marine cyanobacterial natural product curacin A with the colchicine site of tubulin and initial structure-activity studies with analogues. *Mol Pharmacol* 48(3):523–531.
5. Verdier-Pinard P, et al. (1998) Structure-activity analysis of the interaction of curacin A, the potent colchicine site antimitotic agent, with tubulin and effects of analogs on the growth of MCF-7 breast cancer cells. *Mol Pharmacol* 53(1):62–76.
6. Chang Z, et al. (2004) Biosynthetic pathway investigations and gene cluster of curacin A, an antitubulin natural product from the tropical marine cyanobacterium Lyngbya majuscula. *Gene* 67(1):1356–1367.
7. Gu L, et al. (2009) Metamorphic enzyme assembly in polyketide diversification. *Nature* 459(7247):731–735.
8. Miziorko HM (2011) Enzymes of the mevalonate pathway of isoprenoid biosynthesis. *Arch Biochem Biophys* 505(2):131–143.
9. Theisen MJ, et al. (2004) 3-hydroxy-3-methylglutaryl-CoA synthase intermediate complex observed in "real-time". *Proc Natl Acad Sci USA* 101(47):16442–16447.
10. Campobasso N, et al. (2004) *Staphylococcus aureus* 3-hydroxy-3-methylglutaryl-CoA synthase: Crystal structure and mechanism. *J Biol Chem* 279(43):44883–44888.
11. Steussy CN, et al. (2005) X-ray crystal structures of HMG-CoA synthase from *Enterococcus faecalis* and a complex with its second substrate/inhibitor acetoacetyl-CoA. *Biochemistry* 44(43):14256–14267.
12. Skaff DA, et al. (2012) Biochemical and structural basis for inhibition of *Enterococcus faecalis* hydroxymethylglutaryl-CoA synthase, mvaS, by hymeglusin. *Biochemistry* 51(23):4713–4722.
13. Pojer F, et al. (2006) Structural basis for the design of potent and species-specific inhibitors of 3-hydroxy-3-methylglutaryl CoA synthases. *Proc Natl Acad Sci USA* 103(31):11491–11496.
14. Shafqat N, Turnbull A, Zschocke J, Oppermann U, Yue WW (2010) Crystal structures of human HMG-CoA synthase isoforms provide insights into inherited ketogenesis disorders and inhibitor design. *J Mol Biol* 398(4):497–506.
15. Buchholz TJ, et al. (2010) Polyketide β-branching in bryostatin biosynthesis: Identification of surrogate acetyl-ACP donors for BryR, an HMG-ACP synthase. *Chem Biol* 17(10):1092–1100.
16. Calderone CT, Iwig DF, Dorrestein PC, Kelleher NL, Walsh CT (2007) Incorporation of nonmethyl branches by isoprenoid-like logic: Multiple β-alkylation events in the biosynthesis of myxovirescin A1. *Chem Biol* 14(7):835–846.
17. Calderone CT, Kowtoniuk WE, Kelleher NL, Walsh CT, Dorrestein PC (2006) Convergence of isoprene and polyketide biosynthetic machinery: Isoprenyl-S-carrier proteins in the *pksX* pathway of Bacillus subtilis. *Proc Natl Acad Sci USA* 103(24):8977–8982.
18. Haines AS, et al. (2013) A conserved motif flags acyl carrier proteins for β-branching in polyketide synthesis. *Nat Chem Biol* 9(11):685–692.
19. Dutta S, et al. (2014) Structure of a modular polyketide synthase. *Nature* 510(7506): 512–517.
20. Buchholz TJ, et al. (2009) Structural basis for binding specificity between subclasses of modular polyketide synthase docking domains. *ACS Chem Biol* 4(1):41–52.
21. Whicher JR, et al. (2013) Cyanobacterial polyketide synthase docking domains: A tool for engineering natural product biosynthesis. *Chem Biol* 20(11):1340–1351.
22. Dorrestein PC, et al. (2006) Facile detection of acyl and peptidyl intermediates on thiotemplate carrier domains via phosphopantetheinyl elimination reactions during tandem mass spectrometry. *Biochemistry* 45(42):12756–12766.
23. Miziorko HM, Lane MD (1977) 3-Hydroxy-3-methylgutaryl-CoA synthase. Participation of acetyl-S-enzyme and enzyme-S-hydroxymethylgutaryl-SCoA intermediates in the reaction. *J Biol Chem* 252(4):1414–1420.
24. Busche A, et al. (2012) Characterization of molecular interactions between ACP and halogenase domains in the Curacin A polyketide synthase. *ACS Chem Biol* 7(2):378–386.
25. Alekseyev VY, Liu CW, Cane DE, Puglisi JD, Khosla C (2007) Solution structure and proposed domain domain recognition interface of an acyl carrier protein domain from a modular polyketide synthase. *Protein Sci* 16(10):2093–2107.
26. Nguyen C, et al. (2014) Trapping the dynamic acyl carrier protein in fatty acid biosynthesis. *Nature* 505(7483):427–431.
27. Masoudi A, Raetz CRH, Zhou P, Pemble CW, 4th (2014) Chasing acyl carrier protein through a catalytic cycle of lipid A production. *Nature* 505(7483):422–426.
28. Guy JE, et al. (2011) Remote control of regioselectivity in acyl-acyl carrier protein-desaturases. *Proc Natl Acad Sci USA* 108(40):16594–16599.
29. Parris KD, et al. (2000) Crystal structures of substrate binding to *Bacillus subtilis* holo-(acyl carrier protein) synthase reveal a novel trimeric arrangement of molecules resulting in three active sites. *Structure* 8(8):883–895.
30. Simunovic V, et al. (2006) Myxovirescin A biosynthesis is directed by hybrid polyketide synthases/nonribosomal peptide synthetase, 3-hydroxy-3-methylglutaryl-CoA synthases, and trans-acting acyltransferases. *ChemBioChem* 7(8):1206–1220.
31. Miyanaga A, Iwasawa S, Shinohara Y, Kudo F, Eguchi T (2016) Structure-based analysis of the molecular interactions between acyltransferase and acyl carrier protein in vicenistatin biosynthesis. *Proc Natl Acad Sci USA* 113(7):1802–1807.
32. Middleton B (1972) The kinetic mechanism of 3-hydroxy-3-methylglutaryl-coenzyme A synthase from baker's yeast. *Biochem J* 126(1):35–47.
33. Broadhurst RW, Nietlispach D, Wheatcroft MP, Leadlay PF, Weissman KJ (2003) The structure of docking domains in modular polyketide synthases. *Chem Biol* 10(8):723–731.
34. Whicher JR, et al. (2014) Structural rearrangements of a polyketide synthase module during its catalytic cycle. *Nature* 510(7506):560–564.
35. Tang Y, Kim C-Y, Mathews II, Cane DE, Khosla C (2006) The 2.7-Angstrom crystal structure of a 194-kDa homodimeric fragment of the 6-deoxyerythronolide B synthase. *Proc Natl Acad Sci USA* 103(30):11124–11129.
36. Tang Y, Chen AY, Kim C-Y, Cane DE, Khosla C (2007) Structural and mechanistic analysis of protein interactions in module 3 of the 6-deoxyerythronolide B synthase. *Chem Biol* 14(8):931–943.
37. Gu L, et al. (2011) Tandem acyl carrier proteins in the curacin biosynthetic pathway promote consecutive multienzyme reactions with a synergistic effect. *Angew Chem Int Ed Engl* 50(12):2795–2798.
38. Stols L, et al. (2002) A new vector for high-throughput, ligation-independent cloning encoding a tobacco etch virus protease cleavage site. *Protein Expr Purif* 25(1):8–15.
39. Nishihara K, Kanemori M, Kitagawa M, Yanagi H, Yura T (1998) Chaperone coexpression plasmids: Differential and synergistic roles of DnaK-DnaJ-GrpE and GroEL-GroES in assisting folding of an allergen of Japanese cedar pollen, Cryj2, in *Escherichia coli*. *Appl Environ Microbiol* 64(5):1694–1699.
40. Pfeifer BA, Admiraal SJ, Gramajo H, Cane DE, Khosla C (2001) Biosynthesis of complex polyketides in a metabolically engineered strain of *E. coli*. *Science* 291(5509): 1790–1792.
41. Sánchez C, Du L, Edwards DJ, Toney MD, Shen B (2001) Cloning and characterization of a phosphopantetheinyl transferase from Streptomyces verticillus ATCC15003, the producer of the hybrid peptide-polyketide antitumor drug bleomycin. *Chem Biol* 8(7): 725–738.
42. Goldschmidt L, Cooper DR, Derewenda ZS, Eisenberg D (2007) Toward rational protein crystallization: A Web server for the design of crystallizable protein variants. *Protein Sci* 16(8):1569–1576.
43. Kabsch W (2010) Xds. *Acta Crystallogr D Biol Crystallogr* 66(Pt 2):125–132.
44. Winn MD, et al. (2011) Overview of the CCP4 suite and current developments. *Acta Crystallogr D Biol Crystallogr* 67(Pt 4):235–242.
45. McCoy AJ, et al. (2007) Phaser crystallographic software. *J Appl Cryst* 40(Pt 4):658–674.
46. Stein N (2008) CHAINSAW: A program for mutating pdb files used as templates in molecular replacement. *J Appl Cryst* 41(3):641–643.
47. Langer G, Cohen SX, Lamzin VS, Perrakis A (2008) Automated macromolecular model building for X-ray crystallography using ARP/wARP version 7. *Nat Protoc* 3(7):1171–1179.
48. Murshudov GN, Vagin AA, Dodson EJ (1997) Refinement of macromolecular structures by the maximum-likelihood method. *Acta Crystallogr D Biol Crystallogr* 53(Pt 3): 240–255.
49. Painter J, Merritt EA (2006) Optimal description of a protein structure in terms of multiple groups undergoing TLS motion. *Acta Crystallogr D Biol Crystallogr* 62(Pt 4): 439–450.
50. Emsley P, Lohkamp B, Scott WG, Cowtan K (2010) Features and development of Coot. *Acta Crystallogr D Biol Crystallogr* 66(Pt 4):486–501.
51. Chen VB, et al. (2010) MolProbity: All-atom structure validation for macromolecular crystallography. *Acta Crystallogr D Biol Crystallogr* 66(Pt 1):12–21.
52. Schrödinger LLC (2014) The PyMOL Molecular Graphics System, Version 1.7.4.3. Available at www.pymol.org.
53. Eswar N, et al. (2007) Comparative protein structure modeling using MODELLER. *Curr Protoc Protein Sci* 2(2.9):1–31.
54. Sievers F, et al. (2011) Fast, scalable generation of high-quality protein multiple sequence alignments using Clustal Omega. *Mol Syst Biol* 7:539.
55. Waterhouse AM, Procter JB, Martin DMA, Clamp M, Barton GJ (2009) Jalview Version 2–a multiple sequence alignment editor and analysis workbench. *Bioinformatics* 25(9):1189–1191.
56. Adams PD, et al. (2010) *PHENIX*: A comprehensive Python-based system for macromolecular structure solution. *Acta Crystallogr D Biol Crystallogr* 66(Pt 2):213–221.
57. Baker NA, Sept D, Joseph S, Holst MJ, McCammon JA (2001) Electrostatics of nanosystems: Application to microtubules and the ribosome. *Proc Natl Acad Sci USA* 98(18):10037–10041.